Materials and Design 202 (2021) 109527

Contents lists available at ScienceDirect

Materials and Design

journal homepage: www.elsevier.com/locate/matdes

Micro-sized "pelmeni" - A universal microencapsulation approach overview

Valeriya Kudryavtseva [a,b,1], Stefania Boi [c,1], Jordan Read [d], David Gould [d], Piotr K. Szewczyk [e], Urszula Stachewicz [e], Maxim V. Kiryukhin [f,g], Laura Pastorino [c], Gleb B. Sukhorukov [a,h,*]

[a] Nanoforce, School of Engineering and Materials Science, Queen Mary University of London, Mile End Road, London E1 4NS, UK
[b] National Research Tomsk Polytechnic University, 30 Lenin Avenue, Tomsk 634050, Russia
[c] Department of Informatics, Bioengineering, Robotics and Systems Engineering, University of Genoa, Via Opera pia 13, 16145 Genoa, Italy
[d] Biochemical Pharmacology, William Harvey Research Institute, Queen Mary University of London, EC1M 6BQ London, United Kingdom
[e] Faculty of Metals Engineering and Industrial Computer Science, AGH University of Science and Technology, Adama Mickiewicza 30 Avenue, 30-059 Krakow, Poland
[f] Singapore Institute of Food and Biotechnology Innovation, Agency for Science, Technology and Research (A-STAR), 31 Biopolis Way, #01-02 Nanos, Singapore 138669, Singapore
[g] Institute of Materials Research and Engineering, Agency for Science, Technology and Research (A-STAR), 2 Fusionopolis Way, Innovis, #08-03, Singapore 138634, Singapore
[h] Skolkovo Institute of Science and Technology, Bolshoy Boulevard 30, bld. 1, Moscow 143025, Russia

HIGHLIGHTS

- Microencapsulation approach for printed polymer capsules fabrication based on soft lithography method was proposed.
- Polyelectrolyte and polylactic capsules were fabricated to demonstrate the concept.
- Both types of microcapsules have defined torpedo shape and monodispersed size distribution and high loading capacity.
- Wide range of possible cargoes indifferent to its solubility could be encapsulated.

GRAPHICAL ABSTRACT

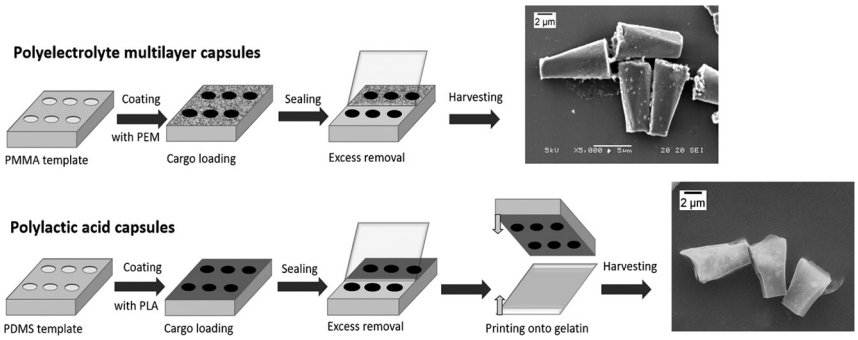

ARTICLE INFO

Article history:
Received 16 September 2020
Received in revised form 17 January 2021
Accepted 24 January 2021
Available online 29 January 2021

Keywords:
Drug delivery
Polymer capsules
Microprinting
Polylactic acid
Soft lithography
Layer-by-layer capsules

ABSTRACT

Microcapsules of customized shapes offer significant advantages over spherical ones, including enhanced internalization by host cells, improved flow characteristics, and higher packing capacity. In our work, we propose a method for defined-shape polymer capsules fabrication inspired by a traditional "pelmeni" (dumplings) making process. The proposed method is based on soft lithography technique. Two different approaches were demonstrated resulting in polyelectrolyte multilayer and poly(lactic acid) (PLA) capsules both showing monodisperse size and shape distribution with about 7 μm long torpedo-like shape. The PLA capsules are described in terms of their morphology, loading of model cargo molecules, cell cytotoxicity and cell uptake. Carboxyfluorescein, $FeCl_2$ ground crystals and Fe_3O_4 nanopowder were used as model cargoes for microcapsules. Capsules demonstrate core-shell structure, high loading capacity, hydrophilic molecules retention and internalization by cells without causing toxic effects. The loading efficiency of model cargo in PLA capsules was more than 80 wt%, resulting in about 40 pg of carboxyfluorescein inside each capsule. Proposed method allows unique advantages compared with alternative microencapsulation techniques, such as precise control over capsules' geometry, flexibility for the choice of active cargoes, regardless of their solubility and molecular weight and potential for triggered release mechanism.

* Corresponding author at: Nanoforce, School of Engineering and Materials Science, Queen Mary University of London, Mile End Road, London E1 4NS, UK.
E-mail address: g.sukhorukov@qmul.ac.uk (G.B. Sukhorukov).
[1] These authors have contributed equally to the study.

https://doi.org/10.1016/j.matdes.2021.109527

1. Introduction

In the last years, strategies for the fabrication of micron and submicron capsules for the encapsulation and controlled release of active substances have received continuous attention [1–3]. In such systems the shell protects and modulates the release of such cargo as enzymes, cells, dyes or drugs for an extensive variety of applications [4,5]. Among the main characteristics of the desired systems should be a high loading capacity and a controllable geometry [6,7]. Ideally, the particle morphology (i.e., size and shape) and composition should be co-designed to enhance the efficiency [8]. Moreover, to promote the in vivo applicability of delivery capsules, they should display biocompatibility, biodegradability, multi-functionality and controlled release by response to internal or external stimuli [9,10].

The synthesis of spherical capsules has been accomplished using different approaches based on hard, soft and self-templating methods [11,12]. However, non-spherical microcapsules [13–16] offer significant advantages over spherical ones, including enhanced internalization by host cells [17–20], improved flow characteristics [21,22], and higher packing capacities [23]. So far, the strategies largely relied on the synthesis or fabrication of colloidal templates followed by their coating with a shell material.

Bottom-up synthetic approach is often used for hard inorganic templates of different shapes. Some recent examples here are anisotropic calcium carbonate microparticles [24,25], iron oxide nanoparticles [18] or cuprous oxide nanocrystals [26]. Porous inorganic templates allow their loading with active substances through various adsorption techniques, where the loading capacity depends largely on the template porosity and molecular weight of the active substance [27]. Low molecular weight molecules adsorb reversibly and their retention in porous templates is very low [28]. For example, the loading capacity of Rhodamine 6G (480 Da) in porous calcium carbonate microparticles decreases from 0.8 to 0.007 wt% after four washing cycles [14]. Macromolecules typically adsorb irreversibly and their loading capacity decreases with molecular weight. Loading capacity of 23 kDa enzyme, guanylate kinase, in porous calcium carbonate of various shapes was ~5 wt%, while a larger 70 kDa dextran demonstrated loading capacity of less than 1 wt % [24]. A more sophisticated approach, freeze-induced loading technique developed recently [29], allows to increase the loading capacity of serum albumin (66 kDa) from 3.7 up to 13.5 wt% after seven consecutive freezing-thawing cycles.

Custom-shaped soft hydrogel templates are fabricated by a variety of top-down techniques [30], e.g. stop-flow lithography [31], drop-on-demand jetting [32]. Microfluidic technologies utilize deformation of liquid droplets under the shear stress of the outer fluids [21,33,34]. A number of approaches towards particles of on-demand shapes exploit Nanoimprint Lithography (NIL): step and flash imprint lithography (S-FIL) [35], subtractive UV-nanoimprint lithography (sUNL) [36], dot-on-pad approach [37] and Particle Replication in Non-Wetting Templates (PRINT) [8,38–40] when templates or molds with variable sizes and shapes were used to produce particles with drugs embedded in their volume. The limitations of these methods include interaction of the active component with liquid precursor and solvents which can lead to its damage and significant diffusive leaching.

A breakthrough in the development of defined-shape capsules with high loading capacities could be the reversing of the typical capsules' engineering process, as shown in the Scheme 1. Stepping away from the traditional core template-based approach allows the entire inner volume of capsules to be available for active compounds loading, while the shell defines capsule's geometry, protects the cargo and modulates its release. Moreover, it offers greater flexibility for the choice of active substances, almost regardless of their solubility and molecular weight, including such sensitive cargoes as sodium percarbonate [41] and hydrophilic peptides [42].

A promising approach to produce defined-shape carriers relies on the fabrication of patterns onto a sacrificial substrate by an appropriate lithographic technique, their templating, subsequent coating with a shell material followed by cargo loading and sealing [43]. This fabrication process results to be fast, highly reusable and potentially applicable to a wide range of polymers, according to the specific requirements.

The approach was first developed for the patterned arrays of microchambers made of polyelectrolyte multilayers (PEMs) [44–46], polyelectrolyte complexes (PECs) [47] or biodegradable materials, such as polylactic acid (PLA) [48], polycaprolactone (PCL) [49] or silk fibroin [50].

In this work, we demonstrate how this process can be modified to produce freely suspended microcapsules of a customized geometry. Two different materials were chosen for the capsules shells. Poly (allylamine hydrochloride)-poly(styrene sulfonate) (PAH-PSS) multilayer film is one of the most common materials in preparing spherical PEM capsules. Polylactic acid (PLA) is a FDA-approved biocompatible and biodegradable polymer and has already demonstrated the ability to block the diffusion of small molecules from microchambers [41,51]. The loading of cargo molecules was obtained by a one-step methods, through powder deposition or in-situ crystallization from concentrated solutions. The capsules harvesting step involves dissolution of a sacrificial template or deposition of gelatin as an anchoring layer, which also possesses surfactant properties preventing aggregation of microcapsules.

The aim of our work is to fabricate capsules with defined shapes exhibiting core-shell structure. We examined this drug delivery system (DDS) by means of scanning electron microscopy, confocal laser scanning microscopy, focus ion beam and investigated cargo loading capacity of the capsules, cell viability and uptake. The proposed capsules could serve various delivery routes including implanted materials, inhaled administration or oral administration [52].

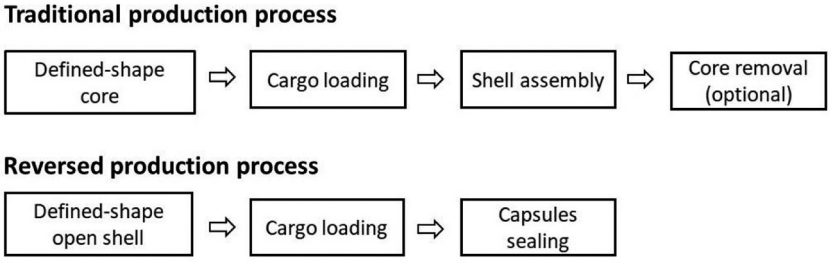

Scheme 1. Traditional vs reversed production process of defined-shape capsules.

2. Materials and methods

2.1. Materials

Polylactic acid (PLA, 3 mm granule) and poly(methyl methacrylate) (PMMA) coil (0.05 mm thick) was purchased from GoodFellow (UK). Gelatin from bovine skin, carboxyfluorescein (CF), Nile Red, Fluorescein 5(6)-isothiocyanate (FITC), DAPI, iron chloride ($FeCl_2$), Iron (II,III) oxide nanopowder (Fe_3O_4 NP), poly(allylamine hydrochloride), Mw = 15 kDa (PAH); poly(sodium 4-styrene sulfonate), Mw = 70 kDa (PSS); branched poly(ethyleneimine), Mw = 25 kDa (PEI), phosphate buffer saline tablets (PBS) were purchased from Sigma-Aldrich and used without further purification. Poly(dimethylsiloxane) kit (PDMS) (Sylgard 184) from Dow-Corning (USA) was used for template fabrication. 1H, 1H, 2H, 2H-perfluoro-decyl trichlorosilane, (>96%) (FDTS) was purchased from Alfa Aesar (Singapore). Sodium chloride, sodium hydroxide, and toluene (ACS grade, anhydrous) were purchased from VWR Singapore Pte. Ltd. (Singapore). Single side polished boron-doped prime silicon wafers (675 μm thick) were purchased from Syst Integration Pte Ltd. (Singapore).

2.2. Microcapsules fabrication

A 2 × 2 cm master silicon mold was purchased from Eulitha AG (Switzerland). The mold's topography was an array of blunted cones 9 μm tall, with 5 μm diameter of the larger base and smaller base shaped as a square having 3 μm edge, as shown in the Fig. 1a. The mold was cleaned in a piranha solution (3:1 mixture of 96% H_2SO_4 and 30% H_2O_2) at 120 °C for 45 min, rinsed with deionized (DI) water, dried in a stream of nitrogen, and placed in a clean oven at 100 °C for 1 h. After that, the mold was treated with a fluoro silane release agent through overnight vapor deposition of FDTS.

In the first approach (Scheme 2a), each PMMA sheet slightly larger than the mold size was placed between the mold and a flat silanized Si substrate and imprinted using Obducat EITRE® Nano Imprint Lithography System (Sweden). The imprinting process was performed at 140 °C and pressure of 4 MPa for 5 min, followed by cooling to 40 °C and releasing the pressure. The imprinted sheets had a negative replica of the mold produced on the PMMA sheet surface, as shown in the Fig. 1b. Layer-by-Layer (LbL) assembly of multilayers was performed by a standard dipping method using a dip-coating robot machine (Riegler & Kirstein GmbH, Germany). Prior to dipping, each imprinted PMMA sheet was sonicated in water in ultrasonic bath for 5 min to remove air bubbles that may be trapped inside the wells. Negatively charged PMMA film was exposed for 15 min to 2 mg/ml PEI hydrochloride solution (pH of PEI solution was adjusted to 5.5 using 1 M HCl) in order to generate the first anchoring layer with high density of positive charges. PSS-PAH coating was produced by alternately dipping the PMMA templates in PSS and PAH solutions of 2 mg/ml concentration at pH ~5.5 and ionic strength 2 M (made with NaCl) for 15 min and three 1 min washings with DI water in-between. The multilayer in-between imprinted wells was gently removed with a tissue paper. Finally, the microcapsules were harvested by dissolving PMMA in toluene and then concentrated by centrifugation followed by two washings with toluene and finally resuspended in water.

In the second approach, (Scheme 2b), patterned PDMS substrate was prepared by casting PDMS pre-polymer and curing agent (10:1 ratio) onto the mold, degassing it for 30 min in vacuum and curing it at 70 °C for 3 h. The substrate was then dipped into 2 *w*/w %. PLA solution in chloroform for 5 s. The solvent was then allowed to evaporate under ambient conditions.

CF, $FeCl_2$ ground crystals and Fe_3O_4 NP were used as model cargoes for microcapsules. Powders were grinded in order to reduce crystals to achieve a more homogeneous filling of capsules lumen. Without this step, bigger crystals were found to affect the capsules shells, thus provoking defects and eventual leakage. Ground powders were then gently spread, onto the open microwells. The excess of powder on the surface of the PDMS stamp was carefully cleaned and swept away with wet fuzz-free lab wipes as described by Zang et al. [49]. The microwells were then successively sealed with a flat PLA layer. The polymer layer in-between the wells was removed with a thin glass slide dipped into solvent and used as a scraper. Following that, the PDMS substrate was printed onto a glass slide covered with 10% gelatin solution in deionized water, and left at −20 °C for 10 min. Given gelatin concentration is sufficiently high to adhere to the microcapsules and, at the same time, it is low enough to allow its dissolution in water in reasonable time. In order to

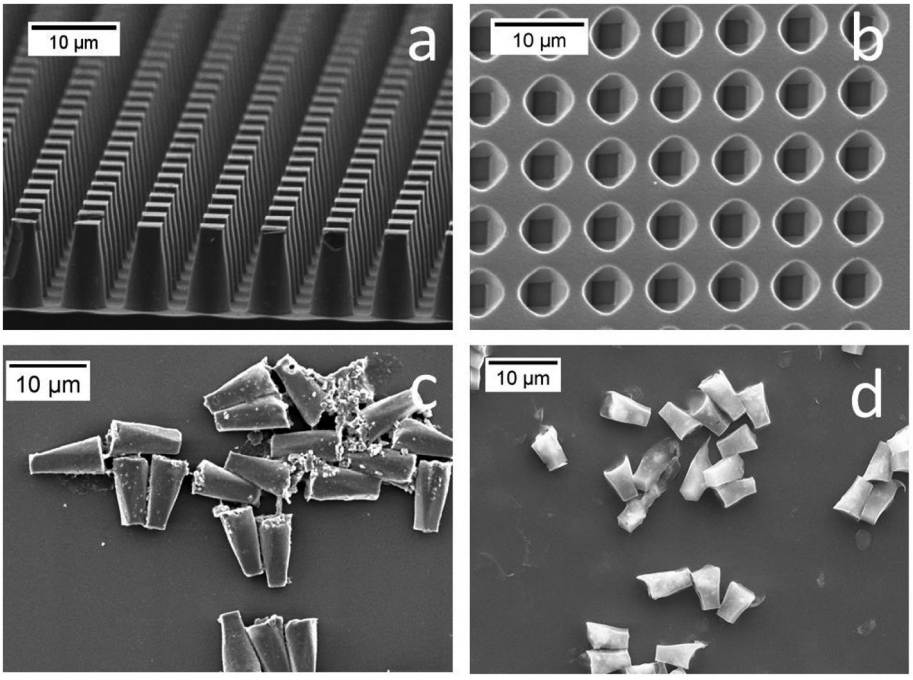

Fig. 1. SEM images of a) micropatterned Si master mold, b) PMMA template, c) PEM microcapsules, and d) PLA capsules.

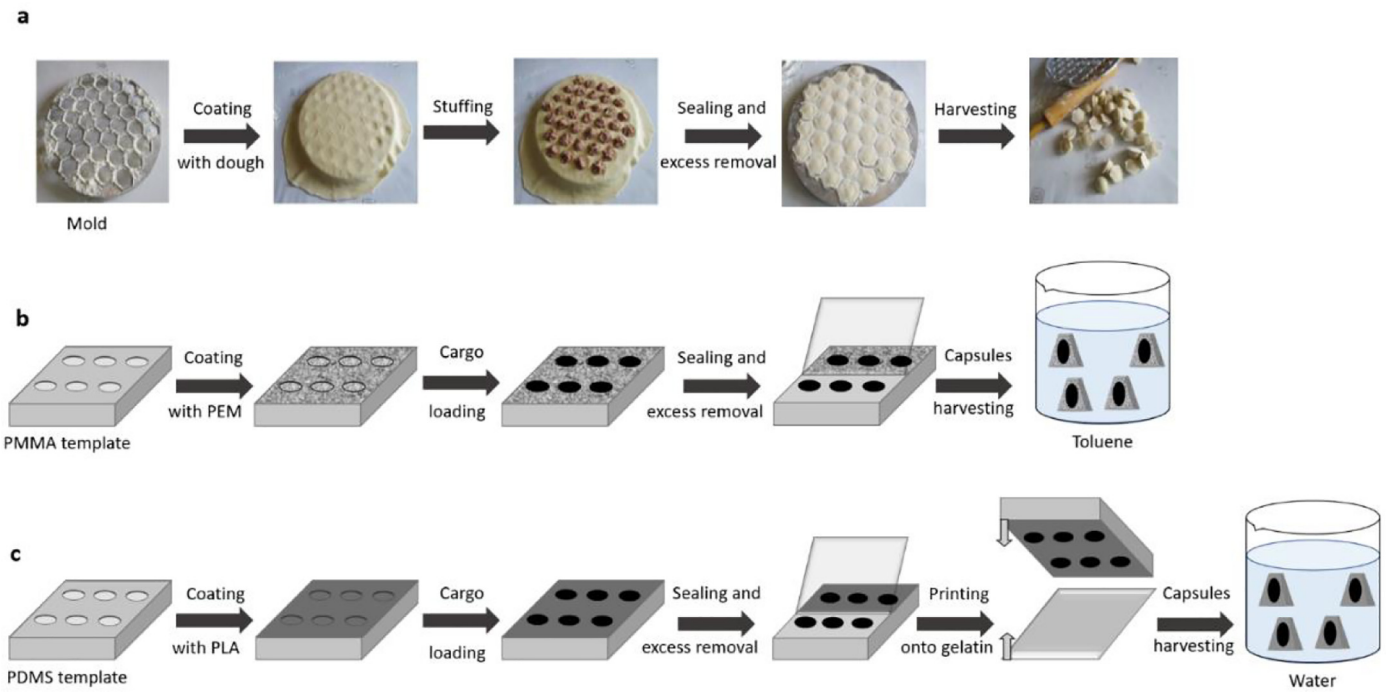

Scheme 2. Schematic illustration of defined-shape microcapsules fabrication. a) Traditional pelmeni production process [53]; b) PEM microcapsules harvesting in toluene; c) PLA microcapsules harvesting in water.

obtain a suspension of microcapsules, gelatin was dissolved in deionized water at 40 °C. The microcapsules were washed three times with warm deionized water by centrifuging them at 7000 RCF for 2 min. The number of capsules after each step was determined with a hemocytometer.

2.3. Microcapsules toxicity for and internalization by HELA- EGFP cells

HeLa EGFP cells [54] were plated in 96-well cell culture plates at a seeding density of 5000 cells per well, in Dulbecco's Modified Eagle Medium (DMEM) supplemented with 10% FCS, 1% L-glutamine and 1% Penicillin-streptomycin (complete DMEM). 24 h after plating, cells were at a density of 10,000 cells per well. Cells were treated, in triplicate, with microcapsules at cell-to-microcapsule ratios of 1:1, 1:3 and 1:10, in a total volume of 100 μl complete DMEM. Control wells contained cells alone. 24 h later, the cells were imaged using an EVOS™ digital colour fluorescence microscope (Thermo Fisher Scientific UK) under phase contrast. Green fluorescent protein (EGFP) and Red fluorescent protein (RFP) channels as well as their overlay was used to assess cell appearance and cell-microcapsule co-localisation. To assess cell viability, the CellTiter-Glo® Cell viability assay (Promega Inc.) was carried out in accordance with manufacturer's instructions. Briefly, 100 μl of CellTiter-Glo® working reagent was added directly to the cell culture plate, without removal of media. Plates were shaken on a rotary shaker for 2 min and allowed to develop for 20 min at room temperature. The entire volume from each well was transferred to a 96-well white polypropylene plate and the luminescent signal in 1 s was recorded using a plate luminometer at a gain of 2000. Wells containing DMEM media + CellTiter-Glo® working reagent were plated as background luminescence control and viability was expressed as a percentage of control cells at each time point.

For cell-microcapsule co-localization HeLa EGFP cells were plated in 12-well cell culture plates in complete DMEM. 24 h after plating, cells were treated with microcapsules loaded with DAPI at cell-to-microcapsule ratios of 1:1 and 1:5. After 24 h of incubation with capsules, cells were fixed with 4% paraformaldehide solution (Sigma Aldrich, UK) and treated with Fluoromount™ Aqueous Mounting Medium (Sigma Aldrich, UK).

2.4. Confocal laser scanning microscopy

Confocal laser scanning microscopy (CLSM, ZEISS LSM710, Germany) was used to visualize gelatin-FITC conjugates onto microcapsules, to investigate the core-shell structure of microcapsules and their internalization with HeLa EGFP cells.

2.5. Characterization of CF encapsulation

The loading capacity of the microcapsules for CF was estimated from the known internal volume of individual microcapsules and the density of CF. It was expressed as a percentage of a control obtained as follows. The PDMS substrate loaded with CF (before the sealing step) was immersed into a PBS 0.01 M.

In order to study the CF release from capsules, samples were placed in PBS solution at room temperature for up to 96 h. 5×10^5 microcapsules were kept into 2 ml 0.01 M PBS. At every time point 0.5 mL of supernatant was taken from microcapsules samples and replaced. The amount of released CF was measured by spectrofluorimetry. Emission spectra were recorded at room temperature using a Perkin Elmer LS55 spectrofluorimeter with Xenon pulsed flash lamp and emission intensity at 490 nm was used. The amount of released CF was calculated from the measured fluorescence values by referring to a previously established calibration curve. All tests were performed in triplicate and the results were expressed as mean ± standard deviation.

2.6. Scanning electron microscopy and cross-sectional imaging

Cross-sectional imaging of capsules was achieved using a dual beam system integrating scanning electron microscope with focused ion beam (FIB-SEM, Quanta 3D, FEI, USA). Prior to microscopy investigation all samples were sputter coated with ~10 nm Au layer (Agar Auto Sputter Coater, Agar Scientific, UK). All cross-sections were prepared and imaged with sample stage tilted to 52° to obtain the 90° angle for FIB milling using Ga- ions at 30 kV accelerating voltage and 50–300 pA current. SEM imaging was accomplished using Secondary Electron (SE) and Backscattered electron (BSE) detectors. BSE detector was used in order

to provide a clear contrast between organic capsule material and a non-organic filler with imaging conditions of 30 kV accelerating voltage and 20–100 μA current. SE imaging was used for morphology investigation at accelerating voltage of 5 kV and 56 μA current. Working distance of 10 mm was used for all FIB-SEM operations.

2.7. Statistics

Statistical analyses were performed in GraphPad Prism, version 8.00 for Windows (GraphPad Software, USA) using one-way ANOVA. Differences were considered significant at the $p < 0.0001$ level.

3. Results and discussion

3.1. Pelmeni-making approach

Scheme 2 shows the fabrication process of freely suspended defined-shape microcapsules, which is further illustrated by scanning electron microscopy (SEM) images in Fig. 1c, d. The process very much resembles making the Russian traditional dumplings, "pelmeni" (Scheme 2a). First, a master silicon mold containing an array of pillars (Fig. 1a) is used to produce a negative replica (an array of microwells) through imprinting on PMMA or PDMS casting (Fig. 1b). Second, a film ("dough") is deposited on the template with an array of wells. Third, a cargo ("stuffing") is put inside each well. Fourth, the wells are sealed with another planar film ("dough") and both films are sealed. Finally, the excess of the film is removed from the template surface and microcapsules ("pelmeni") are harvested.

In this work, we used PAH-PSS multilayer film and PLA film as "dough", corresponding microcapsules are shown in the Fig. 1c-d. In both cases, the microcapsules reproduce the size and shape of the master mold pillars with high fidelity. The capsules' shells are smooth, with no visible pores. An exemplary shape chosen here is high-aspect ratio (~3:1) torpedo-like structure, which has beneficial flow characteristics [21] and enhanced intracellular uptake [17,19,55].

One of the most crucial aspects in designing drug delivery systems (DDSs) is the carrier size, as this parameter can significantly affect drug release profile, injectability and side-effects [56,57]. The height of microcapsules was considered as the indicative parameter for size distributions was found to be narrow with mean 7.15 μm and deviation around 10%. Size and shape of the capsules plays an important role in administration mode, targeting ability and cell internalization [58].

PEM microstructures (microchambers) assembled on patterned templates have several advantages. High robustness in response to mechanical stresses and ability to tailor multiple protective and release-triggering functions are just a few to name [44,46,47]. However, the material is not biodegradable and the process of its assembly is very time-consuming. Contrary, PLA microstructures were shown to be biocompatible, and able to encapsulate low-molecular weight hydrophilic cargoes [48,59,60]. Therefore, PLA capsules were selected to zoom into the process of their formation and encapsulation process.

3.2. Microstructure of sealed PLA capsules

To prepare PLA capsules, a PDMS template was coated with about 0.15 μm thick PLA film stained with Nile Red dye. Microwells were sealed by microcontact printing with a flat PDMS pre-coated with PLA. The film between wells was removed and the capsules were printed onto a glass substrate covered with gelatin-FITC conjugate solution. Gelatin adheres to the PLA capsules, while freezing allows their easy removal from PDMS template. Fig. 2 shows SEM image and 3D CLSM image of obtained array of capsules adhered to gelatin. Fig. 3 shows a series of CLSM images taken upon the capsules harvesting. At first, a layer of gelatin (green colour) is clearly visible on the bottom of capsules (red colour). Upon its dissolution, a thin layer of gelatin is coating the capsules and remains visible even after three washes with 40 °C deionized water. SEM image of the obtained capsules (Fig. 2c) confirms that capsules are well sealed.

3.3. Loading microcapsules with cargo

In this work, the model cargoes were $FeCl_2$, Fe_3O_4 nanoparticles, carboxyfluoresceine (CF) and DAPI.

As iron is an element with high *Z*-number, thus $FeCl_2$ and Fe_3O_4 provide high contrast and can be detected inside the PLA capsules using SEM equipped with backscattered electron detector (BSED). $FeCl_2$ crystals can be clearly seen in most of the capsules, thus demonstrating effective deposition of the powder into PLA-coated PDMS wells. Moreover, defect-free PLA shells effectively prevent water from penetrating inside the capsules upon their harvesting. However, distribution of $FeCl_2$ crystals among the capsules is not homogeneous (Fig. 4 a, b). Possible reason could be a broad distribution of crystal sizes in the $FeCl_2$ powder. Some crystals are up to several micrometers in size, which is comparable to the size of microwells. On the contrary, 20 nm Fe_3O_4 nanopowder crystals fill all available internal volume of the capsules (Fig. 4 c, d) demonstrating high loading efficiency of the proposed encapsulation method.

FIB-SEM in combination with BSE detector allows better visualization of the interior part of the produced capsules. Fig. 5a shows a capsule filled with several $FeCl_2$ crystals, where a free space is evident inside the capsule (red arrows), while Fig. 5b illustrates an even distribution of Fe_3O_4 NP inside capsules and very high-volume fraction of the encapsulated substance. Indeed, even if the shell polymer layer in both cases is shown to be very thin, the smaller Fe_3O_4 crystals allow an almost complete filling of the internal volume.

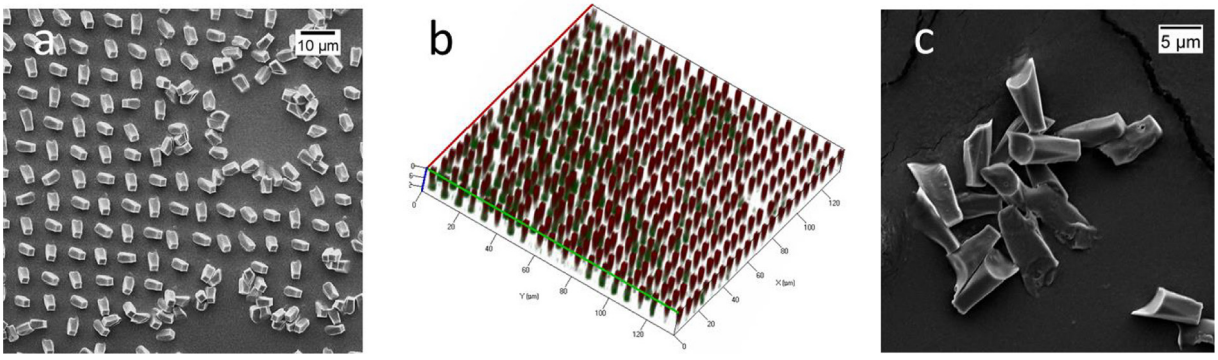

Fig. 2. a) SEM image of PLA printed capsules, b) 3D CLSM image of PLA capsules stained with Nile Red (red) printed onto gelatin-FITC (green); c) SEM images of harvested capsules after washing in deionized water.

Quantitative characterization of the loading capacity (LC) has been achieved with CF. CF has been previously used as model drug to study release and permeability of DDSs [61–63] due to its fluorescence, low molecule weight, water solubility and relative stability. The amount of CF in capsules was measured to be 39.2 ± 5 pg.

The LC was calculated as follows:

$$\mathbf{LC} = \frac{\mathbf{m_{CF}}}{\mathbf{m_{CF}} + \mathbf{m_{shell}}} \cdot 100\% = \frac{\mathbf{m_{CF}}}{\mathbf{m_{CF}} + (\boldsymbol{V_{capsule}} - \boldsymbol{V_{IV}}) \cdot \boldsymbol{\rho_{PLA}}} \cdot 100\%, \quad (1)$$

where $\boldsymbol{V_{IV}}$ is internal volume and $\boldsymbol{V_{capsule}}$ is mean volume of single capsule according to SEM images measurements and $\boldsymbol{m_{CF}}$ is amount of CF per capsules and $\boldsymbol{\rho_{PLA}}$ is standard density of PLA.

The LC of microcapsules is roughly estimated to be 88 wt%, which is much higher than typical microspheres used as an injectable drug depot system [14,24,29,64]. Higher LC allows lower number of capsules needed to achieve required dosage.

The CF was chosen as a model molecule to study release capsules release profile. CF release was performed in PBS solution and was followed up to 96 h (Fig. 6).

Figs. 1d, 2c and 4 demonstrates the production of low-defect containers, the obtained systems enable a prolonged release over time, protecting the carried cargo from the external aqueous environment by PLA hydrophobic shell. However, defects and inhomogeneities in polymer shell formed during the separation step likely affect the encapsulated cargo. The cargo from broken capsule are readily to leak resulting in faster release rates in first hours. The results show higher release rates in first 24 h, corresponding to release from defects and in capsules formed during capsule fabrication. After 24 h the process slowed down and the main contributor to CF release become diffusion from polymer shell. About 18.75% of total CF loaded into capsules according to theoretical calculations was released after 96 h. Therefore, the prolonged cargo release from printed capsules is consistent with the ability of hydrophobic PLA to protect water-soluble molecules inside capsule. Considering PLA is biodegradable polymer, at a longer

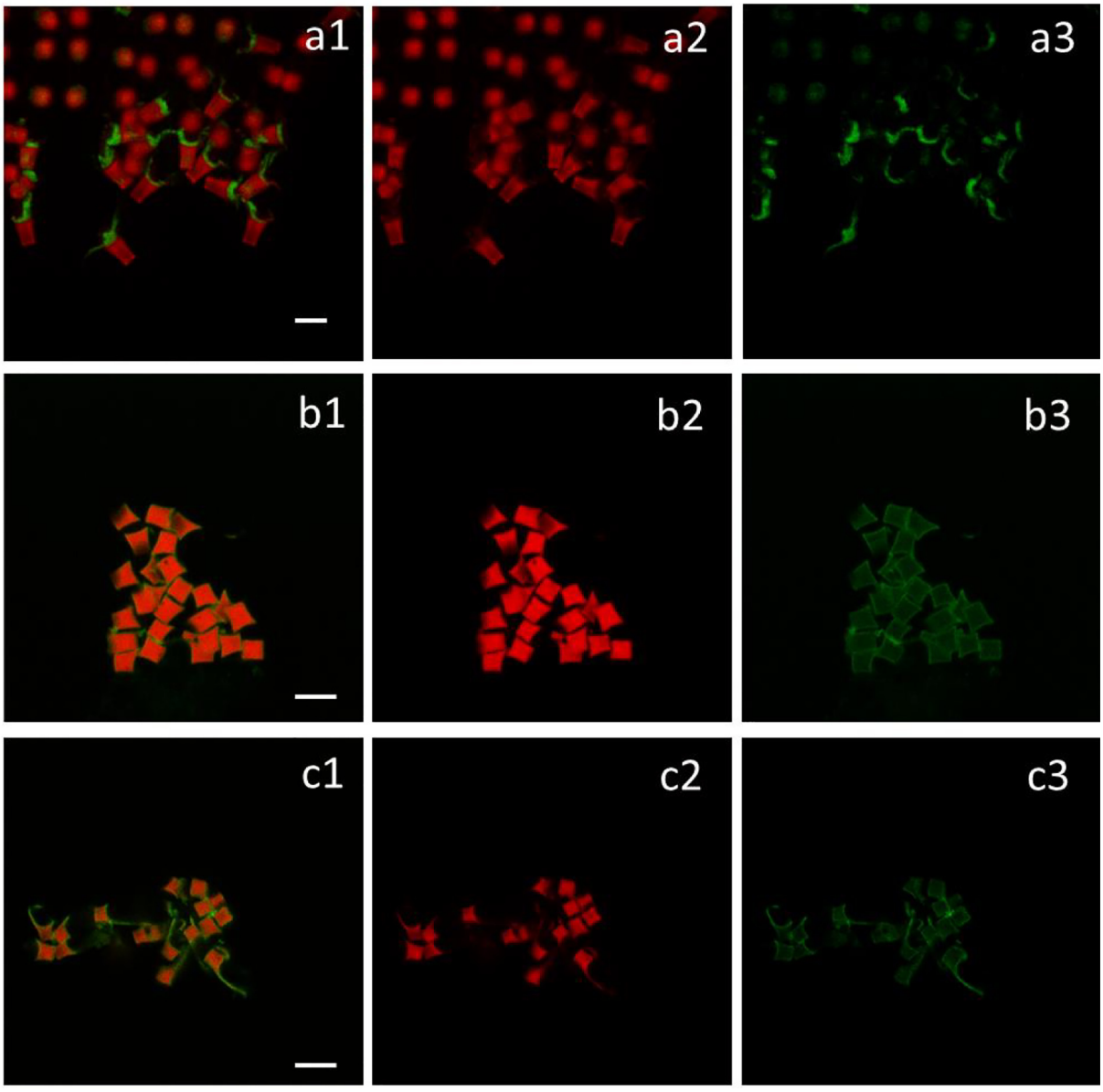

Fig. 3. CLSM images of capsules stained with Nile Red (red) a) printed onto frozen gelatin-FITC (green), b) after gelatin dissolution, c) after washing in deionized water. (1) overlaid image, (2) red channel and (3) green channel. Scale bar is 5 μm.

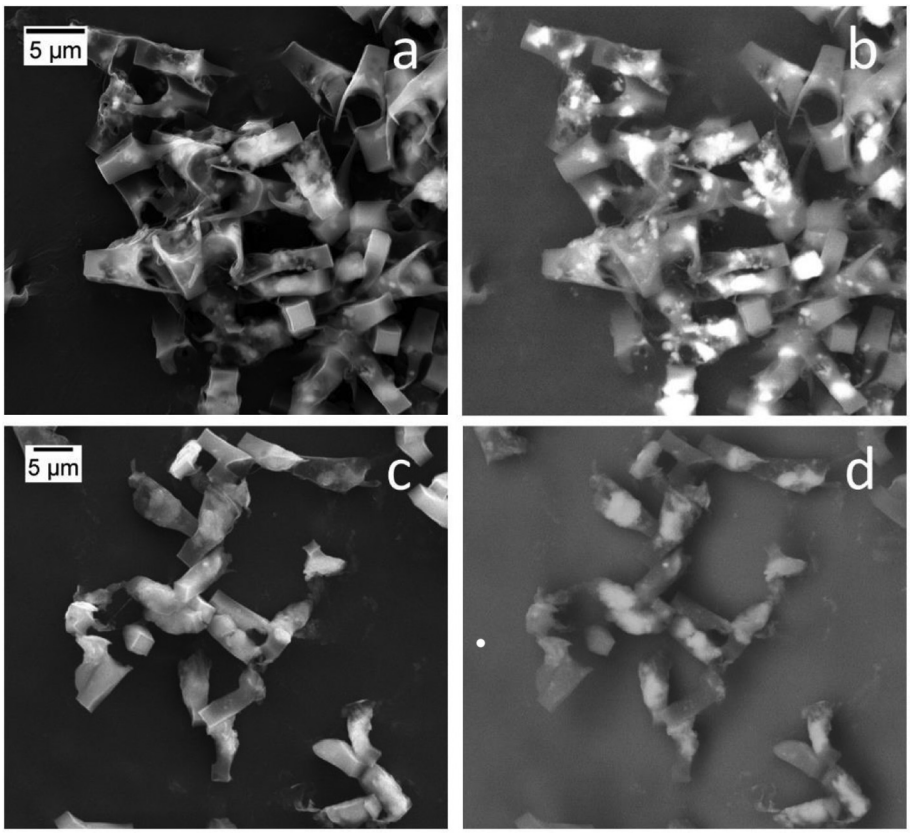

Fig. 4. SEM images obtained with a), c) SE and b), d) BSE detectors in the same area showing the surface morphology and *Z*-contrast of PLA printed capsules loaded with a), b) $FeCl_2$ and c), d) Fe_3O_4 nanopowder.

incubation times higher release rate associated to the degradation of the polymeric capsule will occur. The PLA shell will be slowly decomposed by hydrolysis and the thinnest parts of the shell will form pores leading to higher rates of cargo diffusion [65].

The efficiency of the process could be evaluated as the percentage of capsules from maximum number of capsules that could be produced using the micropatterned template. The efficiency of the process was estimated as ratio of number of capsules after washings against the

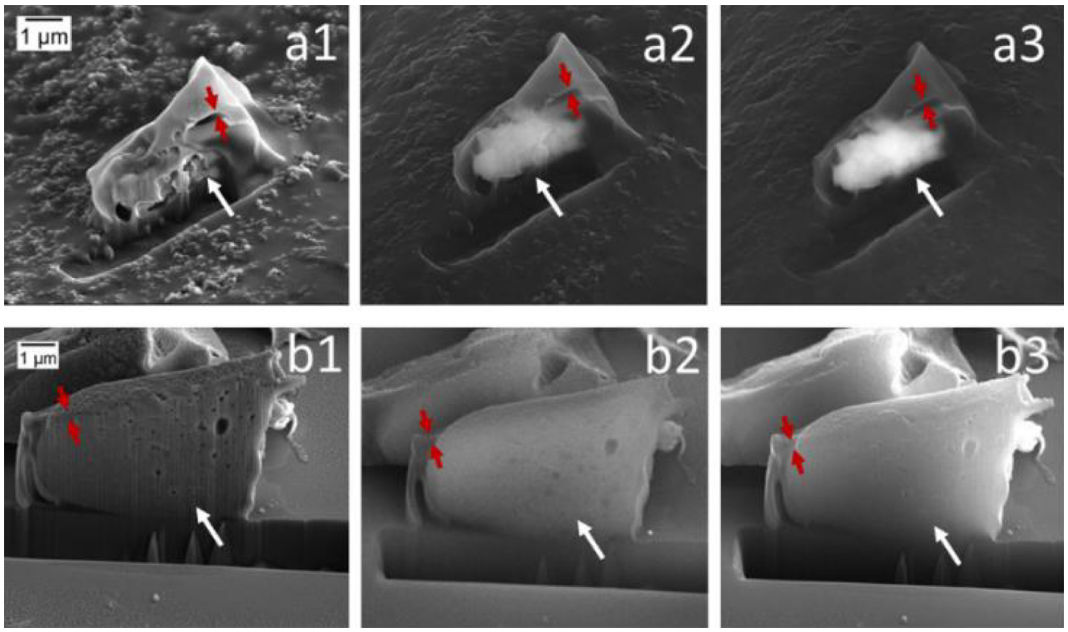

Fig. 5. FIB-SEM cross-sectional image of capsules filled with a) $FeCl_2$ crystals and b) Fe_3O_4 nanopowder obtained with (1) SE, (2) BSE detector and (3) overlaid image. White arrows indicate the cargoes crystals inside the capsules, while red arrows indicate the shell polymer layer.

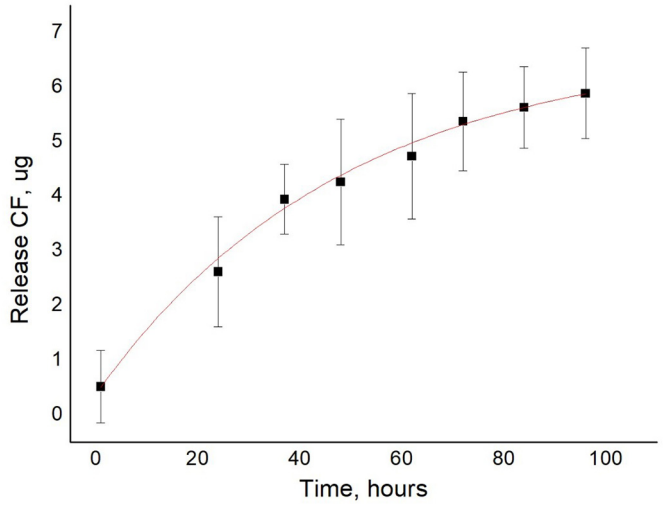

Fig. 6. Release of CF from printed capsules incubated in PBS at room temperature for 96 h. The data are presented as mean ± SD of 3 replicates from one experiment.

number of wells in the template. In our estimation we found about 60% of maximum possible capsules collected after centrifugation washing steps. Few capsules were lost also due to stacking in template and not detaching from gelatine coated substrate.

3.4. Microcapsules uptake and toxicity studies

MTT test was conducted in order to assure that the developed DDSs could be well tolerated by cells. The interaction between HeLa cells and PLA capsules was also studied, as well as the delivery of a model cargo, DAPI to demonstrate the microcapsules' internalization. Cells were incubated with Nile Red labelled capsules at a cell-capsule ratio of 1:1, 1:3 and 1:10 for 72 h.

After incubation for 24 h, intracellular capsule localization was examined using *Z*-stacking in CLSM (Fig. 7). As the encapsulated DAPI is capable of staining alive cells, the blue colour indicates co-localization of cells' nuclei. It was previously shown that layer-by-layer internalized microcapsules are located in cell endosome late developed to lysosomes [66] where pH is acidic. It might cause degradation of PLA and once more defects in capsule structure occur the intracellular leak of DAPI is accelerated. However, small amount of DAPI could be released extracellularly due to capsule's defects and inhomogeneities in polymer shell and DAPI can be uptaken by cells, thus causing the blue staining of the nuclei without capsule internalization. After 24 h in case of 1:1 ratio, capsules were internalized by most of the cells about 0 to 2 capsules per cell, however some of the cells either were unable to uptake or capsules inside were out of the focus of the microscope (Fig. 7a). As shown in Fig. 7b, in case of 1:5 ratio, most cells were associated with internalized capsules and about 3 to 5 five capsules could be found in most of the cells.

The studies showed that ratio of 1 or 3 capsules per cell does not affect cells viability after studied period of incubation. However, at a 1:10 ratio, a statistically significant decrease in cell viability was noticed after 72 h of incubation resulting in 72.1 ± 13.2%, compared to control sample without capsules (Fig. 8). Similar behaviour has been previously reported and it was shown that at high concentration of capsules, capsules trend to sediment on top of the cells responsible for the impairment of the cells and thus decrease cell viability [67,68]. In general, such data demonstrate an excellent biocompatibility of capsules and their negligible cytotoxicity.

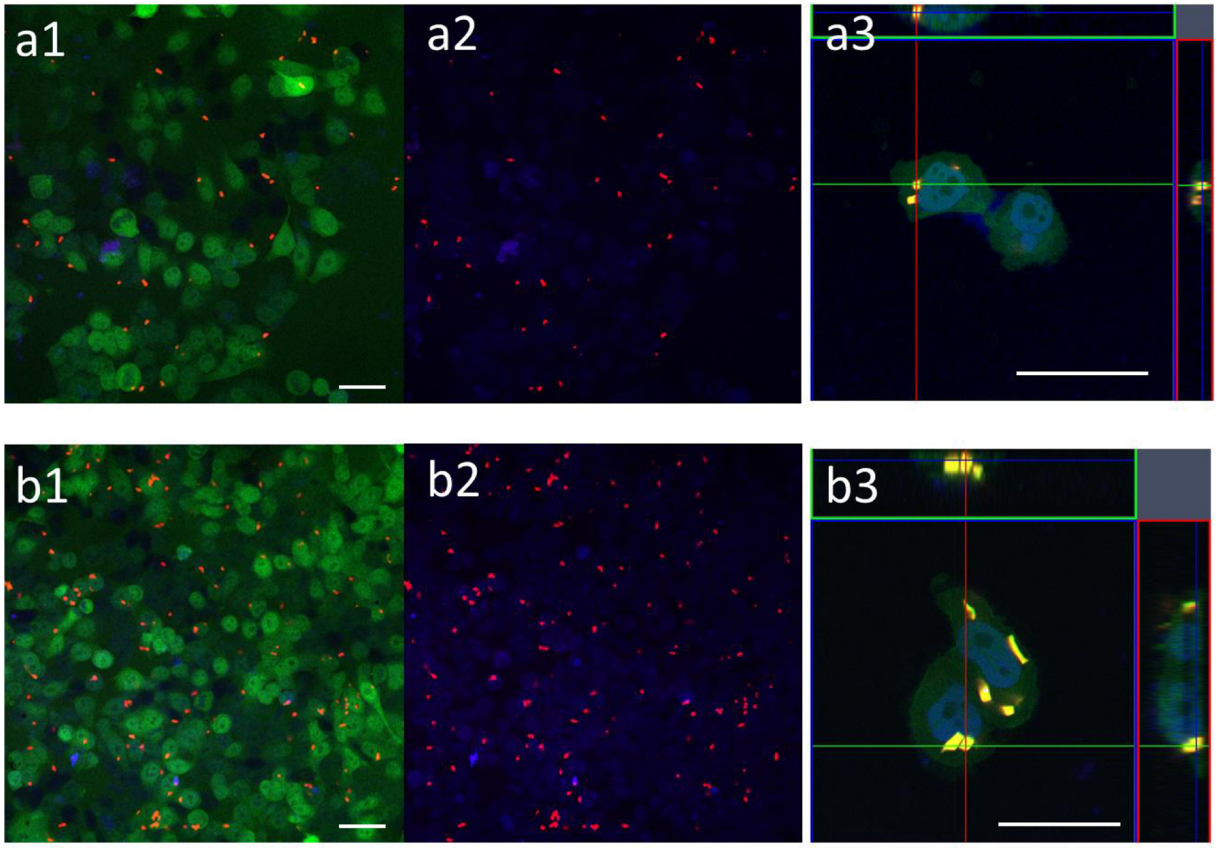

Fig. 7. CLSM images of HeLa EGFP cells (green) incubated for 24 h with Nile red labelled capsules (red) with encapsulated DAPI (blue) at ratio of a) 1:1 and b) 1:5.

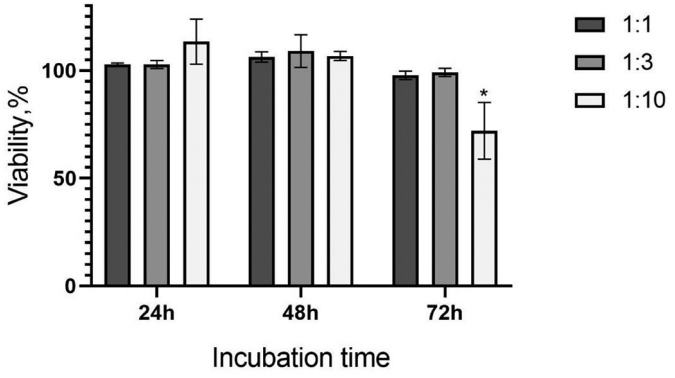

Fig. 8. Results of the HELA EGFP cells Toxicity Test with 1:1, 1:3 and 1:10 cell-capsule ratio. Two-way ANOVA coupled to multiple comparison test, * - $p = 0.0001$.

4. Conclusion

In this paper a traditional approach for dumplings fabrication was adapted for the construction of microsized capsules with high-aspect ratio (~3:1) and torpedo-like shape. Layer-by-layer and biodegradable PLA capsules both showed narrow monodisperse size distribution. Both types could be used for different drug delivery strategies, when the capsule shell defines capsule's geometry, protects the cargo and modulate its release. The proposed DDS was characterized with SEM, FIB and CLSM techniques. Cell viability and internalization were studied. The prepared printed microcapsules exhibit a well-defined core-shell structure, high loading capacity, good cytocompatibility and can be internalized by cells. The LC of the drug in microcapsules was estimated to be 88 wt%, which is much higher than that of similar drug delivery systems. Cell uptake studies underpin the use of our printed capsules for intracellular delivery of therapeutic cargo. Different cargoes were used to explore the DDS encapsulation abilities. The proposed method offers great flexibility for the choice of active substances, regardless of their solubility and molecular weight. The process of encapsulation in proposed printed microcapsules is identical to microchambers with added capsules separation step and harvesting. Currently the entrapment of various cargo in microchambers had been reported including dry powder deposition [49] and precipitation from aqueous solution [69]. It was previously showed that microchambers appear to provide safe loading for sensitive proteins such as neuron growth factor [42]. We assume that sensitive cargo can be successfully encapsulated in proposed capsules as it was reported for microchambers. Additional functionality to the capsules could be tailored by co-encapsulation and surface modification to facilitate their application according to particular needs. The shape of capsules strictly depends on the templates produced by photolithography and various shapes, sizes and aspect ratios of capsules can be achieved according to the needs of application. The main limitations of proposed method are given to photolithography and the thickness of the shell reducing the loading capacity of capsules. Therefore, in case of capsules smaller than thickness of the shell the inner volume might not be enough to accommodate cargo. The process of printed capsules fabrication has a potential for further optimisation to reduce number of lost capsules. The similar processes of shaped solid microparticles scaled-up fabrication were reported via roll-to-roll method [70].

Declaration of Competing Interest

The authors declare that they have no known competing financial interests or personal relationships that could have appeared to influence the work reported in this paper.

Acknowledgments

This project has received funding from the European Union's Horizon 2020 research and innovation programme under grant agreement No. 760827, within the OYSTER project www.oyster-project.eu.

References

[1] A. Larrañaga, M. Lomora, J.R. Sarasua, C.G. Palivan, A. Pandit, Polymer capsules as micro-/nanoreactors for therapeutic applications: current strategies to control membrane permeability, Prog. Mater. Sci. 90 (2017) 325–357, https://doi.org/10.1016/j.pmatsci.2017.08.002.
[2] L.-S. Lin, J. Song, H.-H. Yang, X. Chen, Yolk-shell nanostructures: design, synthesis, and biomedical applications, Adv. Mater. 30 (2018) 1704639, https://doi.org/10.1002/adma.201704639.
[3] M.W. Tibbitt, J.E. Dahlman, R. Langer, Emerging frontiers in drug delivery, J. Am. Chem. Soc. 138 (2016) 704–717, https://doi.org/10.1021/jacs.5b09974.
[4] E.V. Skorb, H. Möhwald, 25th anniversary article: dynamic interfaces for responsive encapsulation systems, Adv. Mater. 25 (2013) 5029–5043, https://doi.org/10.1002/adma.201302142.
[5] R. Jenjob, T. Phakkeeree, D. Crespy, Core–shell particles for drug-delivery, bioimaging, sensing, and tissue engineering, Biomater. Sci. 8 (2020) 2756–2770, https://doi.org/10.1039/C9BM01872G.
[6] Y. Si, M. Chen, L. Wu, Syntheses and biomedical applications of hollow micro-/nanospheres with large-through-holes, Chem. Soc. Rev. 45 (2016) 690–714, https://doi.org/10.1039/C5CS00695C.
[7] X. Wang, J. Feng, Y. Bai, Q. Zhang, Y. Yin, Synthesis, properties, and applications of hollow micro-/nanostructures, Chem. Rev. 116 (2016) 10983–11060, https://doi.org/10.1021/acs.chemrev.5b00731.
[8] J.P. Rolland, B.W. Maynor, L.E. Euliss, A.E. Exner, G.M. Denison, J.M. DeSimone, Direct fabrication and harvesting of monodisperse, shape-specific nanobiomaterials, J. Am. Chem. Soc. 127 (2005) 10096–10100, https://doi.org/10.1021/ja051977c.
[9] A.S. Timin, D.J. Gould, G.B. Sukhorukov, Multi-layer microcapsules: fresh insights and new applications, Expert Opin. Drug Deliv. 14 (2017) 583–587, https://doi.org/10.1080/17425247.2017.1285279.
[10] W. Zhang, T. Ji, Y. Li, Y. Zheng, M. Mehta, C. Zhao, A. Liu, D.S. Kohane, Light-triggered release of conventional local anesthetics from a macromolecular prodrug for on-demand local anesthesia, Nat. Commun. 11 (2020) 2323, https://doi.org/10.1038/s41467-020-16177-w.
[11] C.-H. Ng, N. Rao, W.-C. Law, G. Xu, T.-L. Cheung, F.T. Cheng, X. Wang, H.-C. Man, Enhancing the cell proliferation performance of NiTi substrate by laser diffusion nitriding, Surf. Coatings Technol. 309 (2017) 59–66, https://doi.org/10.1016/j.surfcoat.2016.11.008.
[12] N.A. Feoktistova, A.S. Vikulina, N.G. Balabushevich, A.G. Skirtach, D. Volodkin, Bioactivity of catalase loaded into vaterite CaCO3 crystals via adsorption and co-synthesis, Mater. Des. 185 (2020) 108223, https://doi.org/10.1016/j.matdes.2019.108223.
[13] B. Xue, V. Kozlovskaya, E. Kharlampieva, Shaped stimuli-responsive hydrogel particles: syntheses, properties and biological responses, J. Mater. Chem. B 5 (2017) 9–35, https://doi.org/10.1039/C6TB02746F.
[14] B.V. Parakhonskiy, A.M. Yashchenok, M. Konrad, A.G. Skirtach, Colloidal micro- and nano-particles as templates for polyelectrolyte multilayer capsules, Adv. Colloid Interf. Sci. 207 (2014) 253–264, https://doi.org/10.1016/j.cis.2014.01.022.
[15] L. Huang, K. Wu, X. He, Z. Yang, H. Ji, One-step microfluidic synthesis of spherical and bullet-like alginate microcapsules with a core–shell structure, Colloid. Surf. A 608 (2021) 125612, https://doi.org/10.1016/j.colsurfa.2020.125612.
[16] M. Nowak, T.D. Brown, A. Graham, M.E. Helgeson, S. Mitragotri, Size, shape, and flexibility influence nanoparticle transport across brain endothelium under flow, Bioeng. Transl. Med. 5 (2020) https://doi.org/10.1002/btm2.10153.
[17] X. Liu, H. Zheng, G. Li, H. Li, P. Zhang, W. Tong, C. Gao, Fabrication of polyurethane microcapsules with different shapes and their influence on cellular internalization, Colloids Surf. B 158 (2017) 675–681, https://doi.org/10.1016/j.colsurfb.2017.06.036.
[18] X. Li, M. Bao, Y. Weng, K. Yang, W. Zhang, G. Chen, Glycopolymer-coated iron oxide nanoparticles: shape-controlled synthesis and cellular uptake, J. Mater. Chem. B 2 (2014) 5569–5575, https://doi.org/10.1039/C4TB00852A.
[19] S.E.A. Gratton, P.A. Ropp, P.D. Pohlhaus, J.C. Luft, V.J. Madden, M.E. Napier, J.M. DeSimone, The effect of particle design on cellular internalization pathways, Proc. Natl. Acad. Sci. 105 (2008) 11613–11618, https://doi.org/10.1073/pnas.0801763105.
[20] S. Mitragotri, In drug delivery, shape does matter, Pharm. Res. 26 (2009) 232–234, https://doi.org/10.1007/s11095-008-9740-y.
[21] Q.-W. Cai, X.-J. Ju, C. Chen, Y. Faraj, Z.-H. Jia, J.-Q. Hu, R. Xie, W. Wang, Z. Liu, L.-Y. Chu, Fabrication and flow characteristics of monodisperse bullet-shaped microparticles with controllable structures, Chem. Eng. J. 370 (2019) 925–937, https://doi.org/10.1016/j.cej.2019.03.221.
[22] Y. Geng, P. Dalhaimer, S. Cai, R. Tsai, M. Tewari, T. Minko, D.E. Discher, Shape effects of filaments versus spherical particles in flow and drug delivery, Nat. Nanotechnol. 2 (2007) 249–255, https://doi.org/10.1038/nnano.2007.70.
[23] A. Donev, Improving the Density of Jammed Disordered Packings Using Ellipsoids, Science (80-.) 303 (2004) 990–993, https://doi.org/10.1126/science.1093010.
[24] S. Donatan, A. Yashchenok, N. Khan, B. Parakhonskiy, M. Cocquyt, B.-E. Pinchasik, D. Khalenkow, H. Möhwald, M. Konrad, A. Skirtach, Loading capacity versus enzyme activity in anisotropic and spherical calcium carbonate microparticles, ACS Appl. Mater. Interfaces 8 (2016) 14284–14292, https://doi.org/10.1021/acsami.6b03492.
[25] N. Serov, D. Darmoroz, A. Lokteva, I. Chernyshov, E. Koshel, V. Vinogradov, One-pot synthesis of template-free hollow anisotropic CaCO 3 structures: towards inorganic

shape-mimicking drug delivery systems, Chem. Commun. 56 (2020) 11969–11972, https://doi.org/10.1039/D0CC05502F.
[26] H. Pei, Y. Bai, J. Guo, Z. Gao, Q. Dai, Q. Yu, J. Cui, Tunable morphologies of polymer capsules templated from cuprous oxide particles for control over cell association, Chin. Chem. Lett. 31 (2020) 505–508, https://doi.org/10.1016/j.cclet.2019.04.049.
[27] A. Trofimov, A. Ivanova, M. Zyuzin, A. Timin, Porous inorganic carriers based on silica, calcium carbonate and calcium phosphate for controlled/modulated drug delivery: fresh outlook and future perspectives, Pharmaceutics 10 (2018) 167, https://doi.org/10.3390/pharmaceutics10040167.
[28] B.V. Parakhonskiy, A. Haase, R. Antolini, Sub-micrometer vaterite containers: synthesis, substance loading, and release, Angew. Chem. 124 (2012) 1221–1223, https://doi.org/10.1002/ange.201104316.
[29] S.V. German, M.V. Novoselova, D.N. Bratashov, P.A. Demina, V.S. Atkin, D.V. Voronin, B.N. Khlebtsov, B.V. Parakhonskiy, G.B. Sukhorukov, D.A. Gorin, High-efficiency freezing-induced loading of inorganic nanoparticles and proteins into micron- and submicron-sized porous particles, Sci. Rep. 8 (2018) 17763, https://doi.org/10.1038/s41598-018-35846-x.
[30] X. Fu, J. Cai, X. Zhang, W.-D. Li, H. Ge, Y. Hu, Top-down fabrication of shape-controlled, monodisperse nanoparticles for biomedical applications, Adv. Drug Deliv. Rev. 132 (2018) 169–187, https://doi.org/10.1016/j.addr.2018.07.006.
[31] L. Chen, H.Z. An, P.S. Doyle, Synthesis of nonspherical microcapsules through controlled polyelectrolyte coating of hydrogel templates, Langmuir 31 (2015) 9228–9235, https://doi.org/10.1021/acs.langmuir.5b02200.
[32] Q. Gao, Y. He, J. Fu, J. Qiu, Y. Jin, Fabrication of shape controllable alginate microparticles based on drop-on-demand jetting, J. Sol-Gel Sci. Technol. 77 (2016) 610–619, https://doi.org/10.1007/s10971-015-3890-2.
[33] D. Dendukuri, K. Tsoi, T.A. Hatton, P.S. Doyle, Controlled synthesis of nonspherical microparticles using microfluidics, Langmuir 21 (2005) 2113–2116, https://doi.org/10.1021/la047368k.
[34] Q. Chen, D. Pan, X. Qi, X. Liu, B. Li, Controlled fabrication of solid-shelled capsules with designed geometry sphericity, Chem. Eng. Sci. 208 (2019) 115153, https://doi.org/10.1016/j.ces.2019.08.011.
[35] L.C. Glangchai, M. Caldorera-Moore, L. Shi, K. Roy, Nanoimprint lithography based fabrication of shape-specific, enzymatically-triggered smart nanoparticles, J. Control. Release 125 (2008) 263–272, https://doi.org/10.1016/j.jconrel.2007.10.021.
[36] X. Zhang, Y. Xu, W. Zhang, X. Fu, Z. Hao, M. He, D. Trefilov, X. Ning, H. Ge, Y. Chen, Controllable subtractive nanoimprint lithography for precisely fabricating paclitaxel-loaded PLGA nanocylinders to enhance anticancer efficacy, ACS Appl. Mater. Interfaces 12 (2020) 14797–14805, https://doi.org/10.1021/acsami.9b21346.
[37] P. Zhang, Y. Liu, J. Xia, Z. Wang, B. Kirkland, J. Guan, Top-down fabrication of polyelectrolyte-thermoplastic hybrid microparticles for unidirectional drug delivery to single cells, Adv. Healthc. Mater. 2 (2013) 540–545, https://doi.org/10.1002/adhm.201200200.
[38] S.E.A. Gratton, S.S. Williams, M.E. Napier, P.D. Pohlhaus, Z. Zhou, K.B. Wiles, B.W. Maynor, C. Shen, T. Olafsen, E.T. Samulski, J.M. DeSimone, The pursuit of a scalable nanofabrication platform for use in material and life science applications, Acc. Chem. Res. 41 (2008) 1685–1695, https://doi.org/10.1021/ar8000348.
[39] J.Y. Kelly, J.M. DeSimone, Shape-specific, monodisperse nano-molding of protein particles, J. Am. Chem. Soc. 130 (2008) 5438–5439, https://doi.org/10.1021/ja8014428.
[40] J.L. Perry, K.P. Herlihy, M.E. Napier, J.M. DeSimone, PRINT: a novel platform toward shape and size specific nanoparticle theranostics, Acc. Chem. Res. 44 (2011) 990–998, https://doi.org/10.1021/ar2000315.
[41] A.V. Ermakov, V.L. Kudryavtseva, P.A. Demina, R.A. Verkhovskii, J. Zhang, E.V. Lengert, A.V. Sapelkin, I.Y. Goryacheva, G.B. Sukhorukov, Site-specific release of reactive oxygen species from ordered arrays of microchambers based on polylactic acid and carbon nanodots, J. Mater. Chem. B (2020) https://doi.org/10.1039/D0TB01148G.
[42] O.A. Sindeeva, O. Kopach, M.A. Kurochkin, A. Sapelkin, D.J. Gould, D.A. Rusakov, G.B. Sukhorukov, Polylactic acid-based patterned matrixes for site-specific delivery of neuropeptides on-demand: functional NGF effects on human neuronal cells, Front. Bioeng. Biotechnol. 8 (2020) https://doi.org/10.3389/fbioe.2020.00497.
[43] L.H. Nielsen, S.S. Keller, A. Boisen, Microfabricated devices for oral drug delivery, Lab Chip 18 (2018) 2348–2358, https://doi.org/10.1039/C8LC00408K.
[44] M.V. Kiryukhin, S.M. Man, S.R. Gorelik, G.S. Subramanian, H.Y. Low, G.B. Sukhorukov, Fabrication and mechanical properties of microchambers made of polyelectrolyte multilayers, Soft Matter 7 (2011) 6550, https://doi.org/10.1039/c1sm05101f.
[45] C.M. Andres, I. Larraza, T. Corrales, N.A. Kotov, Nanocomposite microcontainers, Adv. Mater. 24 (2012) 4597–4600, https://doi.org/10.1002/adma.201201378.
[46] M.V. Kiryukhin, S.R. Gorelik, S.M. Man, G.S. Subramanian, M.N. Antipina, H.Y. Low, G.B. Sukhorukov, Individually addressable patterned multilayer microchambers for site-specific release-on-demand, Macromol. Rapid Commun. 34 (2013) 87–93, https://doi.org/10.1002/marc.201200564.
[47] M. Gai, W. Li, J. Frueh, G.B. Sukhorukov, Polylactic acid sealed polyelectrolyte complex microcontainers for controlled encapsulation and NIR-laser based release of cargo, Colloids Surf. B 173 (2019) 521–528, https://doi.org/10.1016/j.colsurfb.2018.10.026.
[48] M. Gai, J. Frueh, T. Tao, A.V. Petrov, V.V. Petrov, E.V. Shesterikov, S.I. Tverdokhlebov, G.B. Sukhorukov, Polylactic acid nano- and microchamber arrays for encapsulation of small hydrophilic molecules featuring drug release via high intensity focused ultrasound, Nanoscale. 9 (2017) 7063–7070, https://doi.org/10.1039/c7nr01841j.
[49] J. Zhang, R. Sun, A.O. DeSouza-Edwards, J. Frueh, G.B. Sukhorukov, Microchamber arrays made of biodegradable polymers for enzymatic release of small hydrophilic cargos, Soft Matter 16 (2020) 2266–2275, https://doi.org/10.1039/C9SM01856E.
[50] C. Ye, D.D. Kulkarni, H. Dai, V.V. Tsukruk, Programmable arrays of "micro-bubble" constructs via self-encapsulation, Adv. Funct. Mater. 24 (2014) 4364–4373, https://doi.org/10.1002/adfm.201400254.
[51] M. Gai, J. Frueh, V.L. Kudryavtseva, A.M. Yashchenok, G.B. Sukhorukov, Polylactic acid sealed polyelectrolyte multilayer microchambers for entrapment of salts and small hydrophilic molecules precipitates, ACS Appl. Mater. Interf. 9 (2017) https://doi.org/10.1021/acsami.7b03451.
[52] V.D. Prajapati, G.K. Jani, J.R. Kapadia, Current knowledge on biodegradable microspheres in drug delivery, Expert Opin. Drug Deliv. 12 (2015) 1283–1299, https://doi.org/10.1517/17425247.2015.1015985.
[53] https://zen.yandex.ru/media/lak_sov/kak-prigotovit-pelmeni-s-pomosciu-metallicheskoi-pelmennicy-5d66133fec575b00ad6de5a3.
[54] J.E. Read, D. Luo, T.T. Chowdhury, R.J. Flower, R.N. Poston, G.B. Sukhorukov, D.J. Gould, Magnetically responsive layer-by-layer microcapsules can be retained in cells and under flow conditions to promote local drug release without triggering ROS production, Nanoscale 12 (2020) 7735–7748, https://doi.org/10.1039/C9NR10329E.
[55] S.E.A. Gratton, M.E. Napier, P.A. Ropp, S. Tian, J.M. DeSimone, Microfabricated particles for engineered drug therapies: elucidation into the mechanisms of cellular internalization of PRINT particles, Pharm. Res. 25 (2008) 2845–2852, https://doi.org/10.1007/s11095-008-9654-8.
[56] F.Y. Han, K.J. Thurecht, A.K. Whittaker, M.T. Smith, Bioerodable PLGA-based microparticles for producing sustained-release drug formulations and strategies for improving drug loading, Front. Pharmacol. 7 (2016) https://doi.org/10.3389/fphar.2016.00185.
[57] J. Xie, L.K. Lim, Y. Phua, J. Hua, C.-H. Wang, Electrohydrodynamic atomization for biodegradable polymeric particle production, J. Colloid Interface Sci. 302 (2006) 103–112, https://doi.org/10.1016/j.jcis.2006.06.037.
[58] J.A. Champion, Y.K. Katare, S. Mitragotri, Particle shape: a new design parameter for micro- and nanoscale drug delivery carriers, J. Control. Release 121 (2007) 3–9, https://doi.org/10.1016/j.jconrel.2007.03.022.
[59] Y. Zykova, V. Kudryavtseva, M. Gai, A. Kozelskaya, J. Frueh, G. Sukhorukov, S. Tverdokhlebov, Free-standing microchamber arrays as a biodegradable drug depot system for implant coatings, Eur. Polym. J. 114 (2019) 72–80, https://doi.org/10.1016/j.eurpolymj.2019.02.029.
[60] M. Gai, M.A. Kurochkin, D. Li, B.N. Khlebtsov, L. Dong, N. Tarakina, R. Poston, D.J. Gould, J. Frueh, G.B. Sukhorukov, In-situ NIR-laser mediated bioactive substance delivery to single cell for EGFP expression based on biocompatible microchamber-arrays, J. Control. Release 276 (2018) 84–92, https://doi.org/10.1016/j.jconrel.2018.02.044.
[61] M. Babincová, P. Sourivong, D. Chorvát, P. Babinec, Laser triggered drug release from magnetoliposomes, J. Magn. Magn. Mater. 194 (1999) 163–166, https://doi.org/10.1016/S0304-8853(98)00553-8.
[62] A. Göpferich, Bioerodible implants with programmable drug release1, J. Control. Release 44 (1997) 271–281, https://doi.org/10.1016/S0168-3659(96)01533-7.
[63] A. Billard, L. Pourchet, S. Malaise, P. Alcouffe, A. Montembault, C. Ladavière, Liposome-loaded chitosan physical hydrogel: toward a promising delayed-release biosystem, Carbohydr. Polym. 115 (2015) 651–657, https://doi.org/10.1016/j.carbpol.2014.08.120.
[64] F. Zabihi, P. Graff, F. Schumacher, B. Kleuser, S. Hedtrich, R. Haag, Synthesis of poly (lactide- co -glycerol) as a biodegradable and biocompatible polymer with high loading capacity for dermal drug delivery, Nanoscale 10 (2018) 16848–16856, https://doi.org/10.1039/C8NR05536J.
[65] T.Y. Lee, M. Ku, B. Kim, S. Lee, J. Yang, S.-H. Kim, Microfluidic production of biodegradable microcapsules for sustained release of hydrophilic actives, Small 13 (2017) 1700646, https://doi.org/10.1002/smll.201700646.
[66] S. Carregal-Romero, M. Ochs, P. Rivera-Gil, C. Ganas, A.M. Pavlov, G.B. Sukhorukov, W.J. Parak, NIR-light triggered delivery of macromolecules into the cytosol, J. Control. Release 159 (2012) 120–127, https://doi.org/10.1016/j.jconrel.2011.12.013.
[67] C. Kirchner, A. Javier, A. Susha, A. Rogach, O. Krefy, G. Sukhorukov, W. Parak, Cytotoxicity of nanoparticle-loaded polymer capsules, Talanta 67 (2005) 486–491, https://doi.org/10.1016/j.talanta.2005.06.042.
[68] C. Kirchner, T. Liedl, S. Kudera, T. Pellegrino, A. Muñoz Javier, H.E. Gaub, S. Stölzle, N. Fertig, W.J. Parak, Cytotoxicity of colloidal CdSe and CdSe/ZnS nanoparticles, Nano Lett. 5 (2005) 331–338, https://doi.org/10.1021/nl047996m.
[69] M. Gai, J. Frueh, V.L. Kudryavtseva, R. Mao, M.V. Kiryukhin, G.B. Sukhorukov, Patterned microstructure fabrication: polyelectrolyte complexes vs polyelectrolyte multilayers, Sci. Rep. 6 (2016) https://doi.org/10.1038/srep37000.
[70] J.M. DeSimone, Co-opting Moore's law: therapeutics, vaccines and interfacially active particles manufactured via PRINT®, J. Control. Release 240 (2016) 541–543, https://doi.org/10.1016/j.jconrel.2016.07.019.